



Remiero

Plasma Electrolytic Oxidation Ceramic Coatings on Zirconium (Zr) and Zr-Alloys: Part-II: Properties and Applications

Navid Attarzadeh 1,20 and C. V. Ramana 1,3,*0

- Center for Advanced Materials Research, University of Texas at El Paso, 500 W. Univ. Ave., El Paso, TX 79968, USA; nattarzadeh@utep.edu
- ² Environmental Science and Engineering, University of Texas at El Paso, 500 W. Univ. Ave., El Paso, TX 79968, USA
- Department of Mechanical Engineering, University of Texas at El Paso, 500 W. Univ. Ave., El Paso, TX 79968, USA
- * Correspondence: rvchintalapalle@utep.edu

Abstract: A plasma electrolytic oxidation (PEO) is an electrochemical and eco-friendly process where the surface features of the metal substrate are changed remarkably by electrochemical reactions accompanied by plasma micro-discharges. A stiff, adhesive, and conformal oxide layer on the Zr and Zr-alloy substrates can be formed by applying the PEO process. The review describes recent progress on various applications and functionality of PEO coatings in light of increasing industrial, medical, and optoelectronic demands for the production of advanced coatings. Besides, it explains how the PEO coating can address concerns about employing protective and long-lasting coatings with a remarkable biocompatibility and a broad excitation and absorption range of photoluminescence. A general overview of the process parameters of coatings is provided, accompanied by some information related to the biological conditions, under which, coatings are expected to function. The focus is to explain how the biocompatibility of coatings can be improved by tailoring the coating process. After that, corrosion and wear performance of PEO coatings are described in light of recognizing parameters that lead to the formation of coatings with outstanding performance in extreme loading conditions and corrosive environments. Finally, a future outlook and suggested research areas are outlined. The emerging applications derived from paramount features of the coating are considered in light of practical properties of coatings in areas including biocompatibility and bioactivity, corrosion and wear protection, and photoluminescence of coatings

Keywords: plasma electrolytic oxidation; biocompatibility; corrosion protection; wear resistance; photoluminescence



Citation: Attarzadeh, N.; Ramana, C.V. Plasma Electrolytic Oxidation Ceramic Coatings on Zirconium (Zr) and Zr-Alloys: Part-II: Properties and Applications. *Coatings* 2021, 11, 620. https://doi.org/10.3390/ coatings11060620

Academic Editor: Małgorzata Norek

Received: 13 May 2021 Accepted: 18 May 2021 Published: 22 May 2021

Publisher's Note: MDPI stays neutral with regard to jurisdictional claims in published maps and institutional affiliations.



Copyright: © 2021 by the authors. Licensee MDPI, Basel, Switzerland. This article is an open access article distributed under the terms and conditions of the Creative Commons Attribution (CC BY) license (https://creativecommons.org/licenses/by/4.0/).

1. Introduction

Plasma electrolytic oxidation (PEO) is a promising electrochemical technique to form ceramic coatings using plasma-assisted oxidation on a broad range of metals, such as Mg, Ti, and Zr [1–3]. The significant merit of this technique is to fabricate protective inorganic layers grown from the substrate with the participation of species from the electrolyte. Forming PEO layers on valve metals boosts surface performances in many applications by enhancing the structural reliability and extending the longevity of functional properties. During the PEO process, the plasma state following extreme voltage and temperature transmits to the surface of the anodic substrate in an alkaline electrolyte and produces inorganic layers with outstanding adhesive strength to the underlayer [4,5]. As asserted unanimously, the PEO technique forms an environmentally friendly, wet-based coating implementing alkaline electrolytes as the primary media and providing conditions for the incorporation of inorganic additives, including silicate, phosphate, aluminate, or organic additives, including sodium oxalate, glycerol to facilitate the physicochemical attraction during the process via electrochemical reactions [6].

Coatings 2021, 11, 620 2 of 18

We explained the paramount roles of the electrical, compositional variables in determining the characteristics of coatings formed during the PEO process. These variables, such as current mode and density, waveform, and duty cycle, would considerably influence the alteration of coatings' surface and composition features. Therefore, earlier studies have been reported to shed light on the effects of PEO parameters on microdischarge characteristics and obtained features of inorganic layers on the Zr and Zr-alloys. Tailoring process variables during the PEO results in improving the applicability and enhancing the functionality of coatings in various aspects. For instance, the excellent corrosion properties of Zr-alloys were attained via controlling both electrical variables and electrolyte composition, which could, in turn, influence the spatial, lifetime, and electrical characteristics of the PEO coatings [7–13]. To the best of our knowledge, no comprehensive review has discussed the applications of the PEO method to prevent degradation, corrosion, and wear, and to improve the biocompatibility of Zr and Zr-alloy extensively. The recent advances in biological responses of Zr implants using the PEO coatings have been reviewed by Fattah-alhosseini's group recently [3]. Furthermore, we presented a detailed review of PEO coatings in Part-I of this issue, where the attention given was on deriving a deeper fundamental understanding of the PEO growth mechanisms and the effect of process parameters on transient discharge behavior at breakdown, initiation, and growth of the oxide layer, and on the incorporation of species from electrolyte. Part-I highlights the fundamental microstructural aspects associated with structural defects, phase transformation, and the role of additives. However, a detailed report on the properties and application of PEO coatings is still missing.

Considering the scarcity of reviews on the PEO coating of Zr and Zr-alloys as a specific group, a comprehensive review is strongly required to provide the integrated perspective on the applicability and performance of PEO coatings respective to current demands in industries, medication, and science. Accordingly, the present review provides the functional features of PEO to approach studying the applicability of coatings with special emphasis on imperative phenomena and applications of interest, such as biocompatibility in medical implantation, extensive endurance of coatings under applied loadings, outstanding protection of underlayer in exposure to corrosive environments, and a broad photoluminescence range. We describe the general picture of structural reliabilities in correspondence with tribological and electrochemical reactions, and the emerging frame of functional properties in a broad range of emitted light is also provided. Finally, future outlook and prospective progress in synergy with enhancing both pre- and post-treatments are given to provide advanced functionality of PEO coatings are outlined.

2. Biocompatibility of PEO Coatings

There is a significant desire to substitute Ti with Zr for surgical implant materials because of lower Young's modulus (92 GPa) compared to titanium (110 GPa), and hence, lower risk for implantation failure due to stress shielding [14,15]. The biocompatibility of Zr is related to the formation of an inherent oxide layer of zirconia, which is bio-inert and restricts its integration with bone tissue during implantation [16]. Therefore, direct bonding with bone and stimulating new bone formation on the Zr surface is not feasible. Besides, the inherent oxide layer with 2 to 5 nm thickness is prone to rupture, erosion, and wear once Zr is employed for high load-bearing implant applications [17,18]. To address these drawbacks, several surface modifications are implemented to boost the bioactivity and corrosion resistance of Zr without compromising its biocompatibility [18–22]. Out of numerous techniques, the PEO process has demonstrated a promising technique to develop firmly adherent, porous, crystalline, relatively rough, and thick oxide coatings on Zr in environmentally friendly alkaline based electrolytes.

Generally, an implant needs to demonstrate outstanding surface features, such as superior bioactivity and biocompatibility. It is expected that implants applicable to dental and orthopedic surfaces demonstrate the capability to facilitate new bone formation and bond steadily and firmly with bone following implantation [23]. The procedure to examine

Coatings 2021, 11, 620 3 of 18

the apatite-forming ability of PEO coatings and Zr substrate is that they are immersed in simulated body fluid (SBF) medium for 14 days, as shown in Figure 1a. After that, the surface can be characterized using techniques, such as scanning electron microscopy-energy dispersive spectroscopy (SEM-EDS), for studying mineralization of the formed apatite layer on the coating surface and checking the elemental composition of the layer. The SEM image illustrated in Figure 1a showed formation of apatite compounds after immersion in SBF for 14 days. Precipitation of compounds composed of Ca and P over the surface was considered the indication of apatite formation. It was evident that sphere-shaped deposits covered the entire surface of all PEO coatings. However, the precipitated layer on the bare Zr surface was not uniform. Elemental analysis showed that the Ca/P ratios of precipitates on PEO coatings were in the range of 1.53 to 1.65, which is close to the stochiometric Ca/P ratio of 1.67 for hydroxyapatite [24].

Yan et al., took advantage of a post-treatment using ultraviolet (UV) irradiation to change the surface chemistry of the PEO coating. It turned out that strong UV irradiation caused the formation of more basic Zr-OH groups on the surface, and, therefore, the hydrophilic nature of the surface improved significantly [25]. Han et al., produced PEO coating containing Ca and P and studied the in-vitro bioactivity, and dominant osteoblast response of the film as a function of the applied voltage ranging from 400 to 500 V [26]. The PEO coating with a predominantly t-ZrO₂ phase could facilitate the accumulation of a more significant quantity of CaO and P compounds at higher applied voltage, while the apatite-forming ability of coatings was also boosted. A facile method to examine bioactivity and biocompatibility of PEO coatings was to study the proliferation and growth feasibility of the attached osteoblast cells on the surface in an alkaline phosphate environment [26]. It was deduced that doping ZrO₂ with Ca²⁺ ions could improve the accumulation of hydroxyapatite (HA) on the ZrO₂ surface. Yan et al., also worked on enhancing the apatiteforming ability by activating the PEO surface using acidic or alkaline solutions. Significant differences in formation of HA on the surface were noticed between the etched PEO surface and intact surface, where HA formed after a short time on the treated surface [27]. Zhang et al., also introduced HA nanorods into the PEO coating via a process in which HA nanorods were prepared via hydrothermal treatment over the PEO coating [28]. The produced calcium partially stabilized zirconia (Ca-PSZ) coating became covered with HA nanorods and showed greater hydrophilicity and apatite-forming ability. That coating was usually prepared in multistep methods or did not contain a crystalline HA layer on the substrates [27,28]. Cengiz et al., prepared a crystalline HA layer using a single-step PEO process on zirconium with enhanced bioactivity [29]. Composition characterization of PEO coatings showed that hydroxyapatite (HA) formed directly in the coating along with calcium zirconium oxide (Ca_{0.134}Zr_{0.86}O_{1.86}) Ca-PSZ and m-ZrO₂. The formation mechanism of the PEO coating with three layers is displayed in Figure 1b. It was found that Ca and P significantly accumulated in the outer region of the coating, while the inner region was rich in Zr and O. The reaction between pre-formed ZrO₂ and Ca²⁺ ions from the electrolyte resulted in formation of the Ca-Zr-O phase in the transition region. After that, high energy sparking regimes during the PEO process could induce HA layer formation, which could be initiated by complex reactions between Ca²⁺ and PO₄³⁻ ions on the anode surface. Thus, coatings with higher wettability could form during the PEO process. Figure 2a,b compares the wettability between the Zr substrate and the modified PEO coating. The formation of hydrophilic HA coating enhanced the wettability and reduced contact angle values in comparison with a bare Zr surface [29].

The crystallinity and morphology of HA phases could play a vital role in cell growth and cell activity [30,31]. Non-crystalline calcium phosphates were not favorable as they might be dissolved in human body fluids, implying instability for implantation [30,32]. Fu et al., studied 3T3 cell proliferation as a marker to test the biocompatibility of PEO coatings. They were able to measure 3T3 proliferation by MTS assay for PEO coatings formed in electrolytes with different KOH concentrations. The cell proliferation ability was enhanced

Coatings 2021, 11, 620 4 of 18

Coatings 2021, 11, 620

significantly after seeding 3T3 cell on the PEO surface, however, the growth rate of 3T3 cells were similar regardless of their formation electrolytes [33].

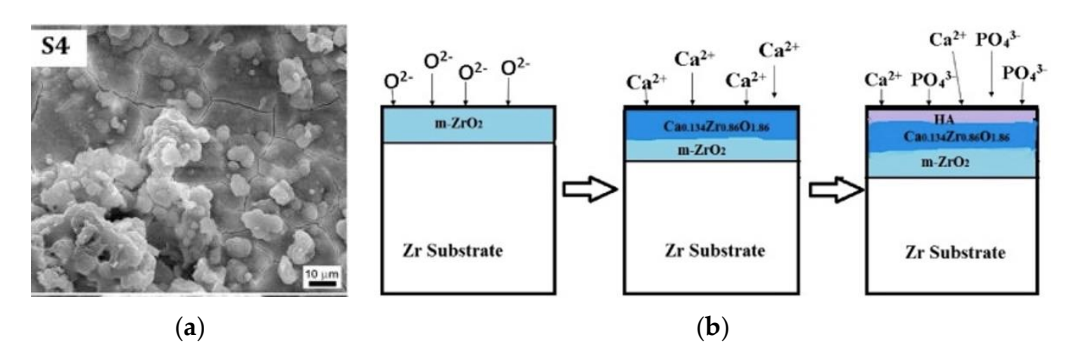


Figure 1: (a) SEM micrographs of the surface of the PEO coating immersed in SBF for 14 days. Figure 1: (a) SEM micrographs of the surface of the PEO coating immersed in SBF for 14 days. Formation of aparticles is the indication of biocompatibility 124] (Reproduced with permission sion number: 504353/087884, Elsevier); (b) schematic representation of the PEO formation containing HA top layer [29] (Reproduced with permission number: 5061321012937, Elsevier). (b) schematic representation of the PEO formation containing HA top layer [29] (Reproduced with permission number: 5061321012937, Elsevier).

The crystallinity and morphology of HA phases could play a vital role in cell growth In contrast to the many efforts to increase biocompatibility of PEO coatings on Zr, and cell activity [30,31]. Non-crystalline calcium phosphates were not favorable as they one of the other aims for surface improvements was to decrease bacterial activity of might be dissolved in human body fluids, implying instability for implantation [30,32], colonization in the vicinity of implants. Antibacterial activity of PEO coatings on It was Fu et al. studied 313 cell proliferation as a marker to test the biocompatibility of PEO coatings for the enhanced by adding silver (Ag), thereby incorporating as an antibacterial agent [34,35], ings. They were able to measure 313 proliferation by MTS assay for PEO coatings formed Fidan et al., produced PEO coatings with silver acetate additives to halt bacterial activities in electrolytes with different KOH concentrations. The cell proliferation ability was enormed the coating of the proliferation of the coatings [36]. Nanoparticles of hanced significantly after seeding 313 cell on the PEO surface, however, the growth rate Ag at concentration below toxicity levels could penetrate environments containing bacteria of 313 cells were similar regardless of their formation electrolytes [33]. As shown in Ag af concentration below toxicity levels could penetrate environments containing pacteria of 3T3 cells were similar regardless of their formation electrolytes [33], and expedite the release of Ag ions, due to the greater specific surface. As shown in In contrast to the many efforts to increase his compatibility of PEO coatings on Zr. Figure 2c, Ag ions demonstrated outstanding antibacterial activity against MRSA as one one of the other aims for surface improvements was to decrease bacterial activity or colorization in the vicinity of implants. Antibacterial activity of PEO coatings on Ti was environed by adding silver (Ag based bioceramic coating, where they deposited hanced by adding silver (Ag), thereby incorporating as an antibacterial agent 134351. Final fine a fining layer of Ag hydrothermally on PEO coated Zr. They found that Ag distributed dan et al. produced PEO coatings with silver acetate additives to halt bacterial activities uniformly profine surface and that the final surface showed hydrophobic nature, in which tof methicillin-resistant Staphulogoccus aureus (MRSA) on the coatings [36]. Nanoparticles the pacterial adhesion of the trial surface reduced significantly compared to the condition of Ag at concentration below toxicity levels could penetrate environments containing bac-without the Ag thin layer [3]. teria and expedite the release of Ag+ ions, due to the greater specific surface. As shown in Aktug et al., produced PEO coatings composed of c-ZrO₂, perovskite-CaZrO₃, and Figure 2c. Age ions demonstrated outstanding antibacterial activity against MRSA as one fet the reconnection after implantation in bioteramic bused and his co-worker also TWEY studied the activisal properties of A.g. based bioseramic coating civilered they deposited. P. dhire layer, P. Agihy, B. Shoring, Syanrelle, Sanco et ede Zalis be interped that Ag. distributed unit MPT massays the sturtage and that the disustage showed hydrongs be states, which the was tarial tedherion of the ifival surface reduced is ignitional to conver and thother condition PEthout the Agthin lawer 637 particular bioselectivity and modified cell-surface interactions. The microbial adhesion decreased with treatment time due to alteration of surface properties in thicker coatings. The difference in cell adhesion activity for Gram-negative and Gram-positive bacteria could be related to difference in cell surface hydrophilicity obtained by the higher amount of HA in prolonged processes [38]. Later, the same research group continued working on the production of PEO coatings containing HA composition to accelerate their interaction and bioactivity once they would be implanted [39].

Cengiz et al., studied the relation between microdischarge types and bioactivity of the PEO coatings for different treatment times ranging from 2.5 to 30 min [40]. The surface characterization revealed that the tetragonal phase formed as the dominant phase during all process times in electrolyte-containing $Ca(CH_3COO)_2 \cdot H_2O$ and $C_3H_7Na_2O_6P \cdot 5H_2O$. It was found that the amorphous HA formed during the PEO process on the coating surface facilitated the formation of HA crystals once coatings were immersed in SBF solution [40]. The combination of the PEO process and electrophoretic deposition (EPD)

Coatings 2021, 11, 620 5 of 18

Coatings 2021, 11, 620

was also implemented to form bioactive ZrO_2/HA composite film [41]. Negatively charged HA nanoparticles were added to phosphate electrolyte to participate in a single-step PEO-EPD process for 2 to 6 min. The coating characterization showed that the uniform and dense ZrO_2/HA coating consisted of c- ZrO_2 and m- ZrO_2 nanocrystalline phases. HA nanoparticles were attracted to the discharge channels due to their charge and entrapped in channels because of the EPD process, while coatings supported greater wettability. After 5 of 19 immersion into SBF for 8 days, an apatite layer covered throughout the surface of ZrO_2/HA coating, indicating considerable modification of in-vitro bioactivity. Besides, it was revealed that the human osteosarcoma could attach, adhere, and propagate considerably on the surface of the ZrO_2 -HA layer, implying the possibility of its implementation as orthopedic in

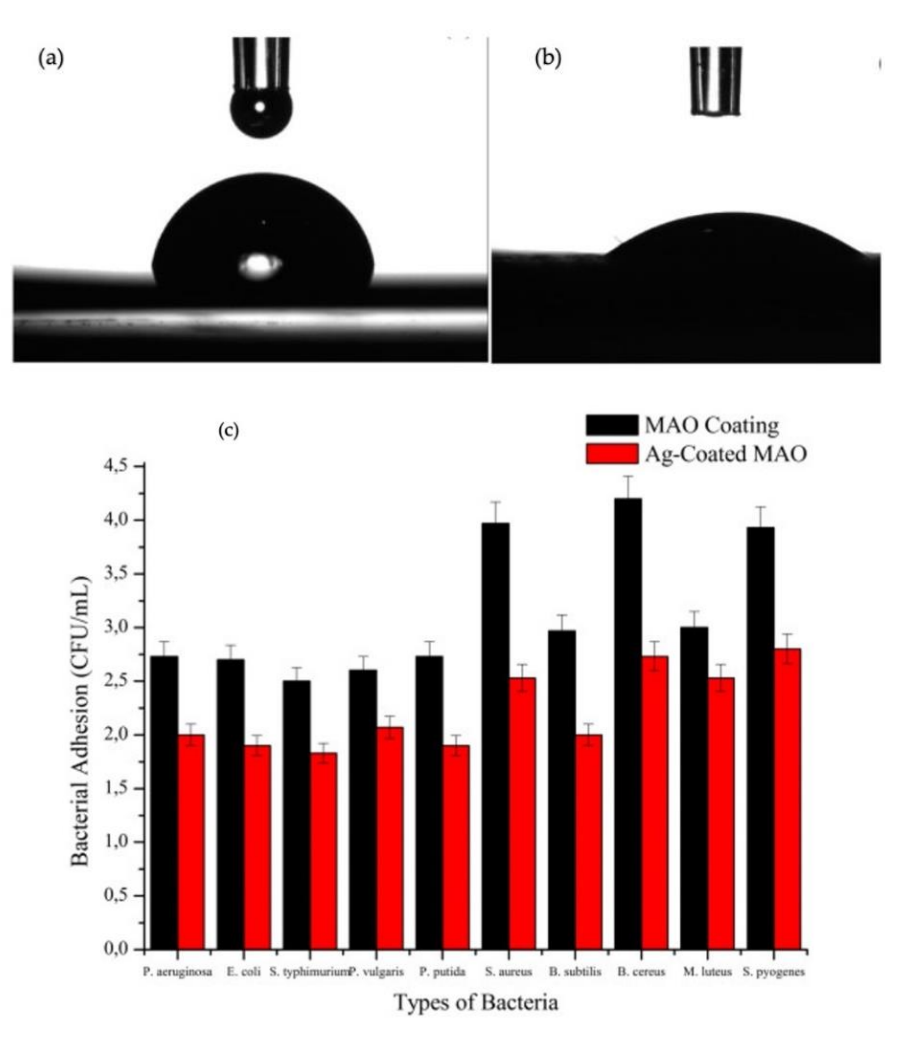


Figure 2.6,16). The worth the context and plane assumements: barressubstrate each the HEPE Octivation of is played, respectively (13912/1849). (Reproduced with the emission number: 506132/102937FIS seivier). (A) alphylotric illustration of a compositive variable for an apositive bacterial's adhesion on the surface of PEO and Agbase 12862 of 13061400310029. Fisseivier)

Acture et al., worked on thermal deposition of the Zn thin film on the PEO coating proActure et al., produced PEO coatings composed of c-ZrO2, perovskite-CaZrO3, and
duced in electrolyte containing calcium acetate and B-CaGP salt [47]. The characterization
hydroxyapatite (14A) in a single step for 5 hat c-ZrO2, CaZrO3, and HX formed to study the
effect of PEO drest mentitipes and a fahrication of particular send have coatingly the positive different positive and Grame propries and because a fahrication of the coatings that the production of t

Coatings 2021, 11, 620 6 of 18

indicating enhanced bioactivity and antibacterial properties for the Zn-deposited PEO coating [42]. Zhang et al., fabricated HA nanorod-patterned zirconia coatings via a hybrid approach [43]. They found that the HA nanorod-patterned coating increased the feasibility of protein absorption and significantly modified the adhesive and proliferative properties of fibroblasts in comparison to untreated coating, suggesting a potential application for percutaneous implants to facilitate the connection to the skin [43]. Recently, Cu was also deposited onto the PEO surfaces without inducing any alteration in surface morphology by using thermal evaporation [44]. Surface characterization revealed the formation of meta-stable calcium zirconium oxide, cubic zirconia, and perovskite calcium zirconate phase. After completing the coating process, coatings with and without Cu top-layer were immersed in simulated body fluid to evaluate their in-vitro bioactivity and antimicrobial properties for Gram-positive and Gram-negative bacteria. Deposition of Cu hydrothermally on the PEO surface enhanced hydrophobic features, where both types of bacteria had a shorter microbial adhesion time to the surface of Cu-deposited PEO coating, thereby suggesting the biomedical application of the surface-modified PEO coating [44].

Very recently, the effect of pore size was studied in PEO coatings with respect to bioactivity and cell interaction properties [45]. Cengiz et al., prepared PEO coatings with various surface morphologies in terms of pore size and surface roughness to investigate in vitro bioactivity and cell interaction features after prolonged immersion in SBF. The in vitro bioactivity evaluations revealed the pore size of the coating significantly affected the growth rate of the HA layer on the coating surface. Remarkably, increasing the pore size promoted HA layer formation in SBF solution, in which higher roughness created by the PEO process increased the chance of HA nucleation, due to boosting the ionic activity of the coating surface [45].

3. Corrosion Resistance Properties

Nuclear grade Zr-alloys like Zircaloy-4 alloy are subjected to neutron irradiation as well as severe conditions of high temperature and high-pressure flowing water [46]. The harsh, aggressive environment exacerbates the corrosion and hydrogen absorption, thus causing fast deterioration of the mechanical strength of structural components [47,48]. Therefore, it is necessary for the nuclear industry to seek methods of curbing the corrosion rate of Zr alloys. On the other hand, Zr and its alloys have recently found a promising application as medical implants. The tendency of implant materials to be subjected to electrochemical reactions within body fluids is crucial to understanding their stability in the human body. Several techniques can be implemented to mimic the situation in the body and study the behavior of coated or noncoated Zr surfaces. Open circuit potential (OCP), Tefel extrapolation, potentiodynamic polarization (PDP), and electrochemical impedance spectroscopy (EIS) are the typical tests carried out on the PEO coated Zr samples to examine their corrosion performance in simulated body fluid (SBF) or other corrosive environments.

The PEO process is identified as a relatively fast, facile, and uncomplicated technique to produce functional ceramic coatings for corrosion-resistant applications on valve metals such as Ti and Zr. It is evident that the corrosion protection of the bare Zr substrate is associated with forming a native oxide layer on its surface. However, this oxide layer is not thick enough (i.e., in the order of a few tens of nanometer) and can be disappeared or degraded in the early stage of load bearing in prolonged applications like medical implants. This ends up raising the corrosion rate, thus reducing the efficacy and service time of the Zr implant. Although PEO coating is an effective method for lowering the corrosion rate due to blocking the charge-transfer mobility across the substrate–environment interface, the PEO coating suffers from its inherited porous nature, where deep pores provide an open path for penetration of aggressive ions and reduction in the overall protection efficiency of coating [9–13,24,49–52]. The PEO coating can form in various electrolytes, such as silicate, aluminate, phosphate, and so on, but all suffer from pancake-like surface features, pores, and cracks [53–55]. The rough and porous surface morphology did not disappear even for procedures without creating pancake-like structures [13,56]. Xue et al., explored the

Coatings 2021, 11, 620 7 of 18

corrosion performance of PEO coating formed in silicate electrolyte using potentiodynamic polarization (PDP) tests [57]. They found that corrosion potentials shifted to more noble potentials and that the corrosion current density dropped several orders of magnitude due to the PEO coating. They claimed thickening the PEO coating impacted the corrosion rate, due to the higher number of cracks [57].

Sandhyarani et al., conducted a series of corrosion experiments to examine the corrosion performance of PEO coatings produced in the phosphate electrolyte with different treatment times. They found that the recorded OCPs of PEO coatings shifted to more noble potentials with a remarkable decrease in $i_{\rm corr}$ compared to that of the untreated Zr sample [12]. No pitting corrosion was observed for the PEO coating produced below 6 min treatment time. However, the PEO coating produced with the longer treatment time (8 min) suffered significant pitting corrosion, which was attributed to numerous cracks on the coated surface. The optimum corrosion performance in SBF environment was recorded for the Zr sample coated up to 6 min, while precipitates were mainly composed of Ca–P rich compounds [12].

The corrosion performance of the PEO coating produced on Zircaloy-4 in the silicate electrolyte using AC regime was tested in nitric acid solution [11]. The authors studied the influence of the frequency of the PEO process on the corrosion resistance of the formed coatings. Electrochemical studies revealed that the performance of coatings produced at both 50 and 100 Hz for 5 and 30 min were similar. No significant difference in the corrosion resistance was found for coatings produced at different frequencies, thus confirming the effect of similar coating morphologies. The Tafel test showed the current density declined remarkably for the PEO coating compared to the bare zirconium, and no noticeable difference was found between coatings with different thicknesses. The authors, therefore, deduced that the main protection was supported by the barrier layer at the base of the coatings [11].

The corrosion performance of PEO coatings produced in $Na_2SiO_3 \cdot 9H_2O$ and KOH solution with 1, 3, 10, and 30 min treatment times was tested in 0.5 M NaCl solution. Among PEO coatings, the coating with 10 min treatment time demonstrated the best corrosion protection properties. Increased porosity was the determining factor in decreasing the corrosion resistance of the PEO coating with 30 min treatment time [51].

Sandhyarani et al., also evaluated the effect of electrolyte composition on the corrosion performance of PEO coatings. They recorded OCP of PEO coatings formed in phosphate and aluminate electrolytes for 4 h and showed OCP values of all PEO coatings tended to more noble potentials, compared to Zr substrate, indicating higher thermodynamic stability of oxide films. At the beginning of immersion, OCP values for PEO coatings showed less noble potential and declined slightly. This instability at the early time of immersion could be associated with an increased activity because of penetration of corrosive solution from surface defects and pores to the metal—oxide interface. The oxide film formed in phosphate and KOH electrolyte showed the highest noble potential values over the entire period of immersion time, which can be related to the modified coating morphology of being pore-free and much smoother than other coatings. However, the film formed in silicate and KOH electrolyte showed higher apatite-forming ability because of superior wettability.

The evaluation of corrosion performance of the PEO composite coatings reiterated the importance of adding nanoparticles, in which the PEO composite coating produced with Ce₂O₃ addition could reduce the corrosion current density about 10³ times compared to the simple PEO coating [9]. Figure 3a shows the polarization curves for the Zr substrate, the simple PEO, and the PEO composite coating with Al₂O₃, CeO₂, or ZrO₂ nanoparticles, termed as PA, PC, and PZ, respectively. Besides, the composite coating of ZrO₂–SiC produced in phosphate electrolyte exhibited superior corrosion resistance compared to coatings produced in aluminate and silicate electrolytes, due to the modified surface morphology of the coating [58].

trolyte. The PEO coating formed in phosphate electrolyte suffered from localized peeling regions caused by stress mismatching of the considerable volume change owing to the transition from tetragonal to monoclinic phases. Figure 3b illustrates the PDP analysis of PEO coatings and the bare Zr substrate, which displayed no passive region for the PEO coatings as a remarkable difference with the bare sample. The corrosion current density three and four orders of magnitude lower than that of the bare electrode for PEO coatings formed in phosphate and silicate electrolyte, respectively.

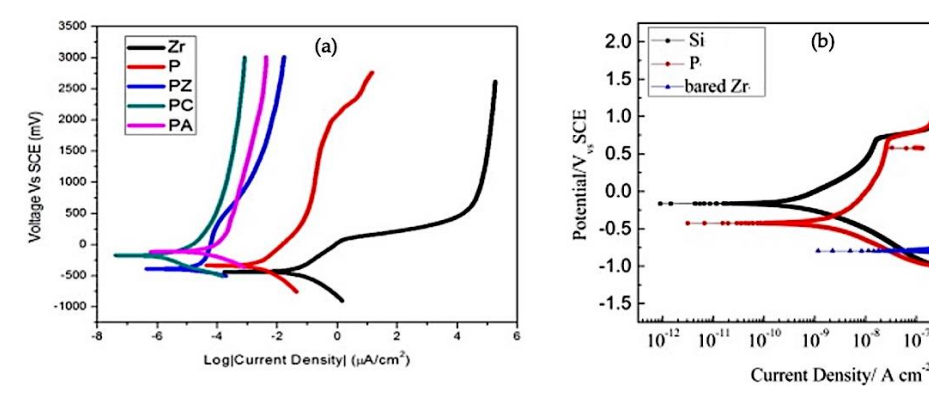


Figure 3: (a) PDP plot of Zr substrate, simple PEO coating (P), composite coating of PEO and each of of Al20, (PA), Ce20, (PC), and ZrO, (PZ) 191 (Reproduced with permission number: 5043540009057 e12503 (PA), Ce20, (PC), and ZrO, (PZ) 191 (Reproduced with permission number: 5043540009057, E12503 (PA), Ce20, (PC), and ZrO, (PZ) 191 (Reproduced with permission number: 5043540009057, E12503 (PC), and Silicate (Si) PEO coatings [39] (Reproduced with permission number: 5043540272527, Elsevier).

10-6

Wang et al., conducted a comparative study on two types of PEO coatings produced on Zircaloy-4 alloy in silicate and phosphate electrolyte. The authors worked on the PDP behaviors and electrochemical impedance spectroscopy (EIS) measurements of PEO coatings immersed in LiOH solution for different time intervals to study the prolonged corrosion performance [59]. The surface morphology of the two coatings showed distinct differences, where the PEO coating formed in silicate electrolyte was more compact, and the population of pores and cracks was fewer than the PEO coating formed in phosphate electrolyte. The PEO coating formed in phosphate electrolyte suffered from localized peeling regions caused by stress mismatching of the considerable volume change owing to the transition from tetragonal to monoclinic phases. Figure 3b illustrates the PDP analysis of PEO coatings and the bare Zr substrate, which displayed no passive region for the PEO coatings as a remarkable difference with the bare sample. The corrosion current density is three and four orders of magnitude lower than that of the bare electrode for PEO coatings formed in phosphate and silicate electrolyte, respectively.

EIS measurements were performed for both coatings immersed in LiOH solution, and various equivalent electrical circuits were suggested to simulate results. Figure 4a,b shows the Nyquist plots of EIS results for silicate and phosphate coatings, and Figure 4c,d shows the suggested electrical circuits for prolonged immersions. It was evident that the silicate coating with modified surface morphology could endure the aggressive condition greater and protect zirconium more significantly in the long-term immersion process.

Li et al., mixed graphene oxide (GO) particles into silicate and a mixture of phosphate and silicate electrolytes to produce the PEO composite coatings of zirconia with graphene on N36 Zr alloy [8]. They studied corrosion and fretting behavior of the composite coating and investigated the influence of GO addition on improving the corrosion resistance. The authors reported the positive role of GO particles in enhancing the anti-corrosion behavior of PEO coating, in which the coating formed with 0.1 g/L GO at silicate electrolyte exhibited the best corrosion performance. The GO particles developed a good barrier against penetration of aggressive ions and blocked access to the substrate [8]. Very recently, the same authors compared the corrosion performance of PEO composite coating with each of Al₂O₃, MoS₂, CeO₂, and graphene oxide (GO) on Zr alloy [7]. The positive effect of adding nanoparticles was to lower the corrosion current density with more noble corrosion potential due to impeding aggressive ions before they reach the substrate.

Wu et al., combined the PEO process with pulsed laser deposition (PLD) to enhance the corrosion protection of composite film formed on Zr-4 alloy [60]. PLD was used to form a $Cr/CrN/Cr_2O_3$ film covering the PEO coating to boost the corrosion resistance of the film on Zr alloy. The EIS study confirmed improving the corrosion resistance via enlarging the polarization resistance, suggesting contribution of dense $Cr/CrN/Cr_2O_3$ film on the corrosion performance of ZrO_2 film though blocking ion attacks more effectively.

EIS measurements were performed for both coatings immersed in LiOH solution, and various equivalent electrical circuits were suggested to simulate results. Figure 4a,b shows the Nyquist plots of EIS results for silicate and phosphate coatings, and Figure 4c,d shows the suggested electrical circuits for prolonged immersions. It was evident that the silicate coating with modified surface morphology could endure the aggressive condition greater and protect zirconium more significantly in the long-term immersion process.

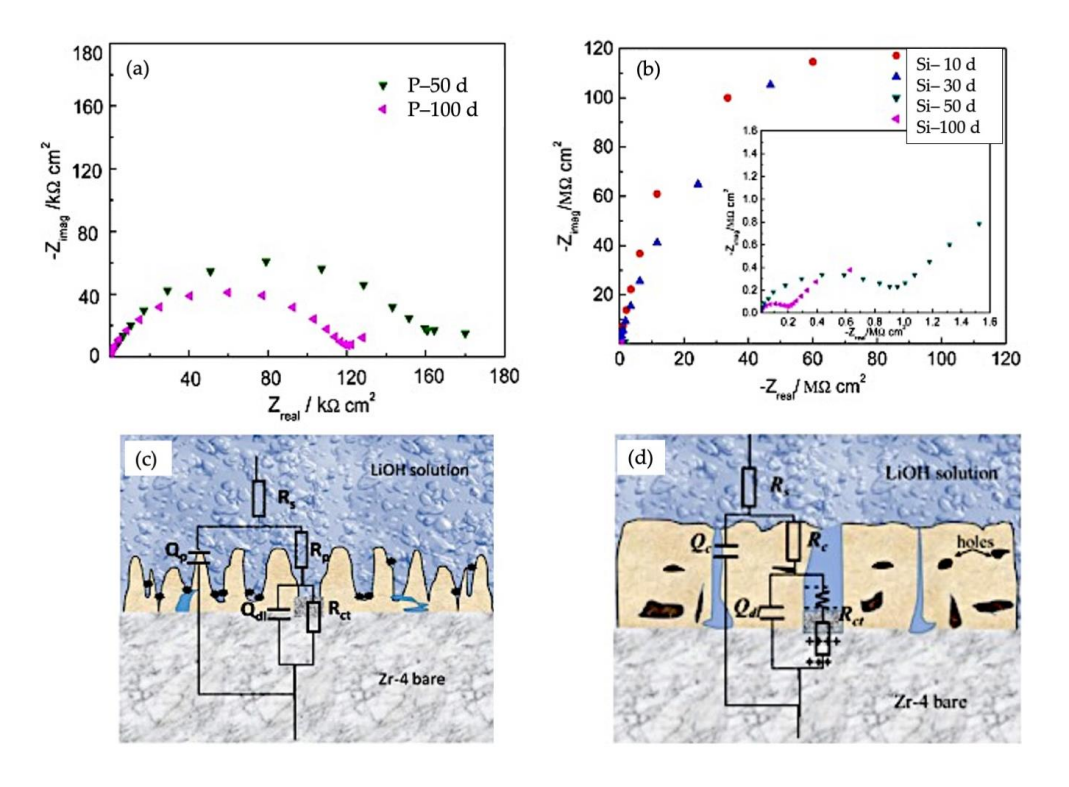


Figure 4. (a,b) Nyquist plots of ElS results of phosphate and silicate ESC continuous for broughed immersions, executively 1589 (cd) diquivalent nice with a halprical an addition of probate and silicate PEACC DECORDANCE and an additional silicate probability of probability of

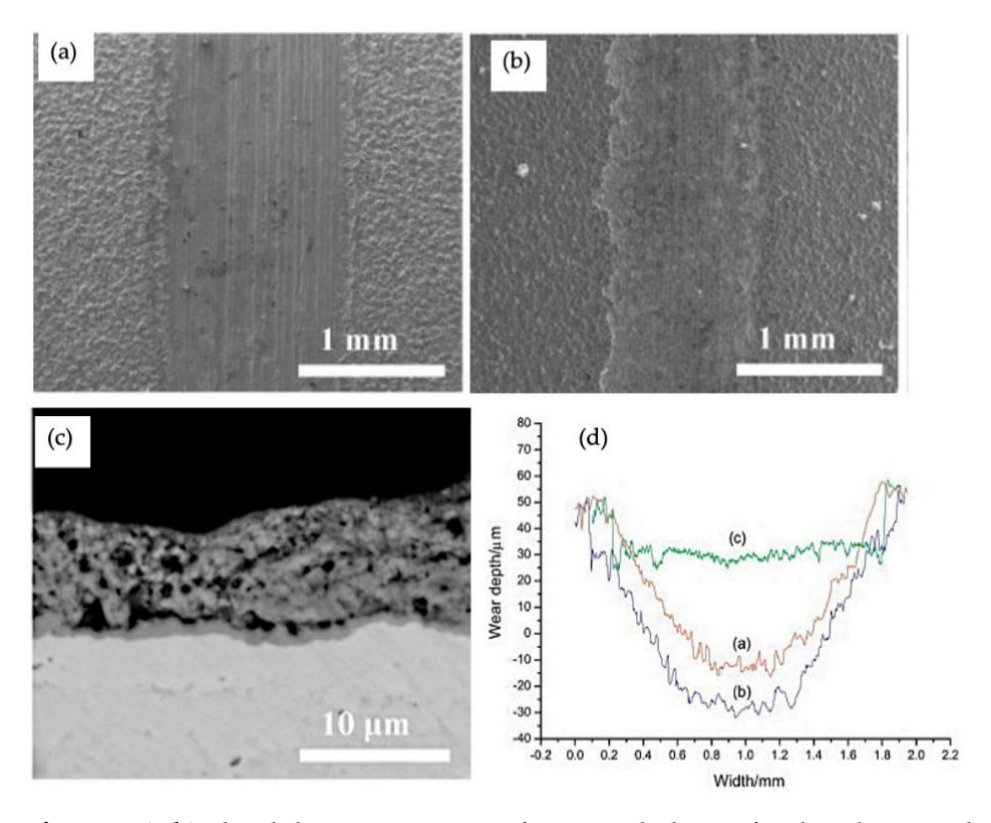
4. Weat and Tribology aphther Exals (acting articles into silicate and a mixture of phosphate and Italians the motor than the properties and the position of the properties and the position of the position o

Cheng et al., performed dry sliding wear tests using an applied load of 10 N for coatings produced for 5, 10, and 30 min in dilute electrolyte of aluminate and KOH [54]. The friction coefficient of the PEO coating formed for 5 min ranged from \sim 0.13 to \sim 0.17 during 240 s of the sliding test; a continuous rise was then observed in the friction coefficient after the initial low values, which could indicate substrate removal. During the initial stage of testing, the very low friction coefficient was driven by the modified morphology of the coating. It was found that the PEO coating formed for 10 min showed weaker wear protection under the same load. The large gap (\sim 20 µm) between the inner layer and the

Coatings 2021, 11, 620 10 of 18

outer layer caused the weak tribological behavior. The transition point (end of coating life) for the coating formed for 10 min occurred much faster than the coating formed for 5 min. Finally, the friction coefficient of the coating formed for 30 min rose significantly from \sim 0.4 to \sim 0.67 during 344 s as the initial stage of testing. After that, the coefficient remained constant until \sim 1252 s, and then abruptly declined to the lowest value of \sim 0.47 at 1394 s. Figure 5d displays the profile along the cross-sections of the wear scars after the dry sliding tests for coatings produced with different PEO treatment times. The weakest wear performance with the deepest scar was observed for the PEO coating produced for 10 min due to the early collapse of the compact outer layer, and thus exposing the thin inner layer. The greatest wear performance was recorded for the coating formed for 30 min with a wear depth of \sim 20 μ m.

Coatings 2021, 11, 620



Figigure (5.6) at h) There idipagtion partaen resurfactor of proof problem is a temperate of the respectively. Contents a second the respectively of the respective of t

The surface cross-section image of the wear scar remained after dry sliding wear test for the PEO coating produced in aluminate electrolyte for 30 min were shown in Figurable. PEO coating produced in aluminate electrolyte for 30 min were shown in what it has produced in aluminate electrolyte for 30 min were shown in what it has been been into the distributed of the shown in the coating produced in aluminate electrolyte for 30 min were shown in what it has been been been electrolyte for 30 min were shown in what it has been been electrolyte for 30 min were shown in the was intended should be shown the intended should be shown the intended as the straint of the shown the product of the sliding during the remained on the wear track. The patches with the transfer layer produced above the surrounding inner layer and supported the contact points with the straint steel ball. The patches with the transfer layer produced above the surrounding inner layer and supported the contact points with the steel ball. The remained on the wear track. The provided shows the surrounding inner layer and supported the contact points with the steel ball. The remained should be previous. The provided shows the surrounding inner layer and supported the contact points with the steel balls. The remained should be previous the surrounding the sliding process and acted as lubrication [65] aliding wear tests were also performed on the coatings formed in concentrated alumelectrolyte [54]. Furthermore, the PEO coating formed for 10 min in concentrated alumelectrolyte [54]. Furthermore, the PEO coating formed for 10 min in concentrated alumelectrolyte [54]. Furthermore, the PEO coating formed for 10 min in concentrated alumelectrolyte [54].

nate electrolyte with the thickness of ~64.4 µm was tested under a high load of 30

Coatings 2021, 11, 620 11 of 18

concentrated aluminate electrolyte [54]. Furthermore, the PEO coating formed for 10 min in concentrated aluminate electrolyte with the thickness of \sim 64.4 μ m was tested under a high load of 30 N and compared with the coating formed in dilute aluminate electrolyte for 30 min with a thickness of \sim 75.8 μ m. Figure 6c,d demonstrate the cross-sectional profiles of wear scars due to the dry sliding test for 30 min for comparing PEO coatings formed in concentrated and dilute aluminate electrolyte and for comparing PEO coatings formed in aluminate and phosphate electrolyte [54]. The low friction coefficient at early times could be related to lack of formation of the transfer layer on the coating surface; however, developing the transfer layer due to frictional heating and mechanical stresses caused the friction coefficient to rise [66]. Cheng et al., finally concluded that the PEO coating formed for 10 min demonstrated greater wear protections, while the wear depth was \sim 20 μ m after 30 min of dry sliding with the applied load of 30 N.

12 of

Coatings **2021**, 11, 620

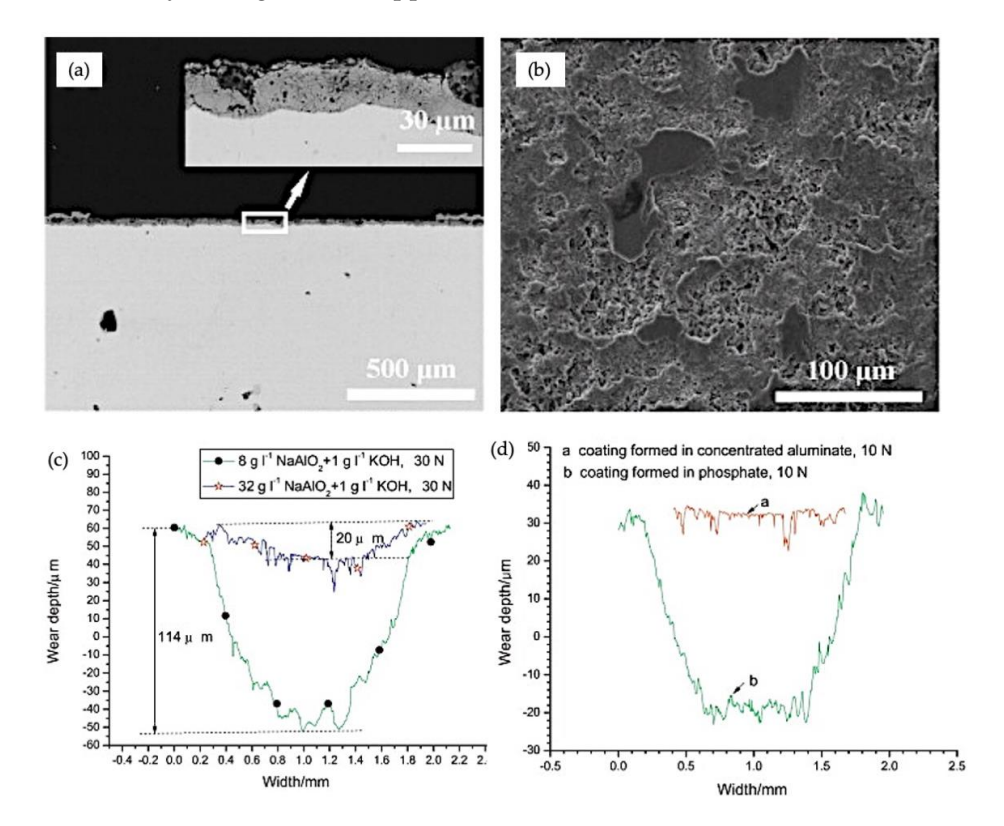


Figure 6a) The recrease in a control of the learnest in the control of the property of the property of the period of the period

The presence of nanoplate-like \(\alpha = \text{Al}_2 \text{O}_3 \) out-layered \(\alpha \text{I}_2 \) out-layered \(\alpha \text{I}_2 \) out-layered \(\alpha \text{I}_2 \) of the presence of nanoplate-like \(\alpha = \text{Al}_2 \text{O}_3 \) out-layered \(\alpha \text{I}_2 \) of the presence of nanoplate-like \(\alpha = \text{Al}_2 \text{O}_3 \) out-layered \(\alpha \text{I}_2 \) of the presence of the wear protection of PEO coating significantly \(\alpha \text{I}_3 \), highlighting its potential applicability for articular head replacement of two found that the presence of the property of the property of the presence of the property of the presence of the property of the presence o

the adhesive wear, where the substrate demonstrated the abrasive wear [69]. Adding gr phene oxide (GO) particles in electrolyte also showed a positive effect on reducing friction

Coatings 2021, 11, 620 12 of 18

Zirlo alloy in similar conditions, and the wear mechanism of PEO coating was primarily the adhesive wear, where the substrate demonstrated the abrasive wear [69]. Adding graphene oxide (GO) particles in electrolyte also showed a positive effect on reducing friction and improved the fretting wear resistance [8]. The PEO coating with GO addition showed delamination, wear debris, and channel trace, demonstrating abrasive wear as the dominant wear mechanism. However, the PEO coating with GO did not show worn-out protrusion in the surface morphology. Recently, Li et al., conducted a comparative study on the influence of different nanoparticles, including Al₂O₃, MoS₂, CeO₂, and graphene oxide (GO), on fretting corrosion behavior [7]. Basically, the nanoparticles embedded in coatings acted as a lubrication phase to decrease the friction. The composite PEO coatings with MoS₂ and GO showed low coefficient of friction value in the initial stage of the wear test, after detaching the nanoparticles, the coefficient of friction rapidly increased. It was suggested that abrasive wear was the main wear mechanism for the PEO coating with Al_2O_3 , while the wear mechanism for the PEO coating with either MoS_2 or CeO_2 was abrasive wear and adhesive wear. For the PEO coating with GO, the wear mechanism was abrasive wear. The PEO composite coating with GO showed that the wear volume was lowest among other composite coatings, but its tribocorrosion performance revealed the highest material loss due to the impact of wear during the corrosion test. The presence of GO particles could effectively reduce the friction and wear as GOs had small shear stress between the layers making the sliding process easier.

5. Photoluminescence Performance

 ZrO_2 based materials have drawn considerable interest from many researchers in photonics, optoelectronics, and electronics due to their outstanding thermal, mechanical, electrical, and optical properties [70–73]. Optical transparency in the visible and near infrared region, high refractive index, low optical loss, wide energy bandgap (\sim 5 eV), and low phonon frequency (\sim 470 cm $^{-1}$) have demonstrated zirconia as a potential matrix host for fabrication of doped compounds using highly efficient luminescent materials ranging from rare-earth to transition metals [74–79]. Recently, researchers have intended to take advantage of PEO processing to entrap rare-earth oxide particles in the ZrO_2 matrix [74–81].

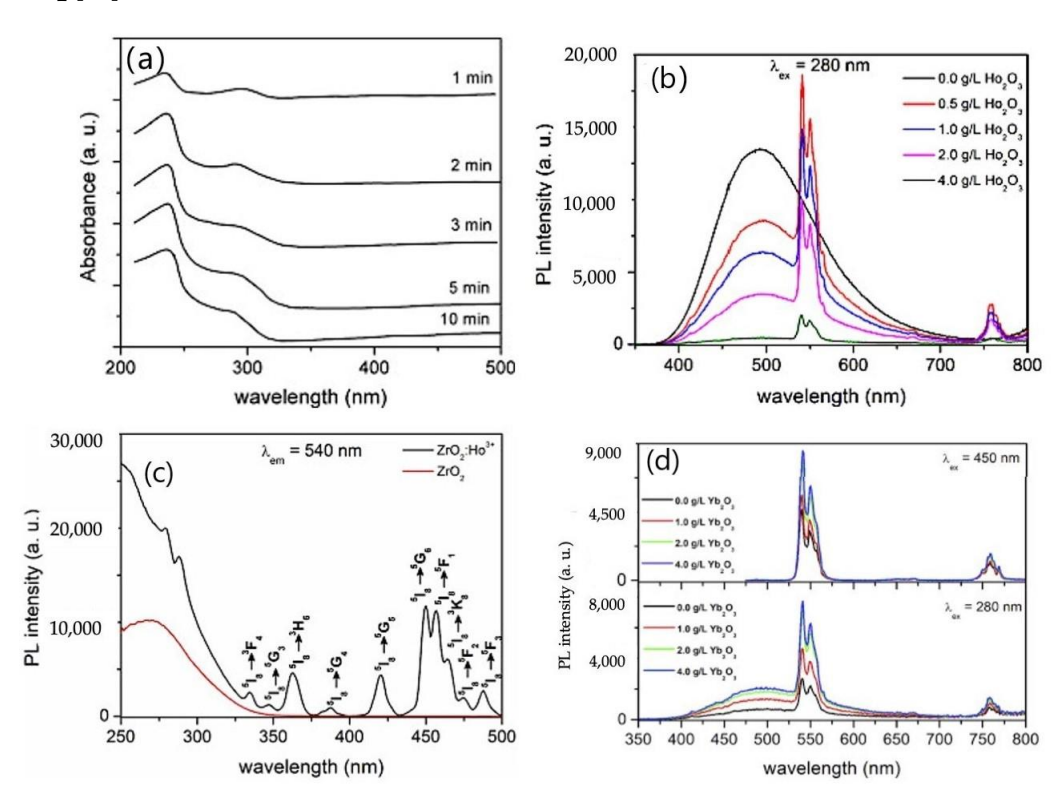
Figure 7a demonstrated diffuse reflection spectra of the PEO coating produced in citric acid electrolyte for a range of treatment times from 1 to 10 min [82]. A wide absorption band was detected spanning the range of 200 to 330 nm. The main absorption peak occurred at approximately 236 nm (~5.2 eV in photon energy) that could be related to photon excitation from valance band to conduction band [83,84]. In addition, the absorption peak at approximately 294 nm (~4.3 eV in photon energy) could be related to the interstitial Zr³⁺ ions [85]. Photoluminescence (PL) measurements displayed easily identifiable PL bands ranging from 300 to 600 nm at ambient temperature. The emission spectra divulged 4 peaks centered approximately at 418, 440, 464, and 495 nm. The prolonged PEO treatment time increased the PL intensity because the concentration of oxygen vacancies enhanced in m-ZrO₂ films, which was responsible for PL excitation bands. This behavior was also recorded for photocatalytic activity of zirconia films, in which prolonged PEO treatment time enhanced the activity as a result of entrapping more oxygen vacancies in the thicker film [82]. Stojadinović et al., worked on the possibility of fabricating doped ZrO₂ coatings with Ho³⁺ and Ho³⁺/Yb³⁺ using the PEO process in phosphate electrolyte containing Ho₂O₃ or H₂O₃/Yb₂O₃ particles [78]. They investigated up- and down-conversion PL properties of the complex oxide coatings composed of ZrO₂ as a host and rare-earth oxide as components of the composite. Notably, rare-earth oxide particles featured zeta potentials in the negative range for alkaline environments, and thereby, the applied potential in the PEO process sucked Ho₂O₃ and Yb₂O₃ particles toward the anode and entrapped them inside microdischarge channels to form a composite of mixed oxides [78]. The PL emission spectra of PEO coatings evolved with different quantities of Ho₂O₃ particles and excited with 280 nm radiation, as illustrated in Figure 7b. Pure ZrO₂ coating could only display a wide PL band with a spectral maximum approximately at 490 nm in the visible

13 of 18 Coatings 2021, 11, 620

14 of 19

Coatings 2021, 11, 620

region originating from optical transitions in PL centers derived from oxygen vacancies of ZrO₂ [82].



Fibigre 97 (44) Alteration of diffuse a delition approximation film films have treatment that of the PED process[82] (Reproduced with principal on unhabe 945434343698 Fisely (b) photoluminecessore amission spectra excited with 2200 mm addition of APCO coar producted in phosphoto hate elektribblyteewiikhaalddittion off Http: 03ppowder in different concentrations for a tweatmoon tition coff 10 mili [78];[6];photalatalineinescenes citationspeptra of and pedantil Ho-doped ZrO2 coatings prodepreduce PEOFED for restreatmentation of a aminim phosphate extertoblete with tandard with the 2/3-g/L HbbQQadditition[178]; (d) photohuninesseen consission specket excited 2014n2815 and 43 dintionadiation BEPEO tingtipgs chroding himphate phate differ with ted it in additing / If 410291. Hat i Desparticles and Mag Particultic less differing the contraction of the street times of ither of 10% hills of 50% less different contractions from an treet times of ither of 10% hills of 50% less different contractions are successful. with representations bear 150 4255 50 4255 50 0 E265 1 pt lsevier).

Therefore, two overlapping regions could be found in down-conversion PL spectra. Therefore, two overlapping regions could be found in down-conversion PL spectra of the composite coating excited by 280 nm including the broad PL bond from the matrix of the composite coating excited by 280 nm including the broad PL bond from the matrix and several emission bands related to 1-f transition of Ho³ ions [78]. At around 540 and and several emission bands related to 1-f transition of Ho³ ions [78]. At around 540 and 550 nm, there were two predominant peaks relating to F₄ 57. 55th non-there iwere twee productions of the peaks of the processing ranged in Sensity in transitions wide positively black of the Etopen RED aprobe than a probe that the Etopen RED aprobe that the entire the entire than t theowide of this siturband partner Platithen Bit vinter bit ZnOs gratier and under partner the genission bothered is the convertation of the theory and in the strategies of the strategies o where higher concentration of his ion hand, indicating the three zeros of a non-radiative ducing the PE intensity of the broad emission band, indicating the presence of a non-radiative at 540 nm for both doped and un-doped zirconia coatings, as shown in Figure 7c. While energy transient between matrix and dopants [78]. The PL excitation spectra were rectine excitation PL spectrum of un-doped zirconia depicted a wide band centered at about 7. orded at, 540 nm for hoth doped and dup-doped zirconia continues an intensified wide ure 7c. While the excitation of interest in darket process and solution of the control of about 1280stribettheen it it it is a specific of the control of th wiides bahtbitanging ation 250 tee 325 broadedese benal, shaip speaks peeks ween 325 aandt 500 nm. Electron retation between ground state the production of the Eronafold 4P orisitals of Handiassissed of Internitation it in the Early by different bind; swifted in the reference the Perelated to direct excitation from ${}^{5}I_{8}$ ground state to the greater energy level of the 4f-manifold. Peaks and assigned electronic transition are clearly illustrated in Figure 7c. Therefore, the PL emission intensity of doped zirconia coatings with rare-earth ions could alter with changing the thickness of the PEO coatings and concentration of rare-earth ions particiCoatings 2021, 11, 620 14 of 18

emission intensity of doped zirconia coatings with rare-earth ions could alter with changing the thickness of the PEO coatings and concentration of rare-earth ions participating in the composite coating [78]. The down-conversion PL emission spectra of PEO coatings formed in electrolyte containing H_2O_3 and different concentrations of Yb_2O_3 particles are also shown for excitements at 280 and 450 nm radiations in Figure 7d. The addition of Yb^{3+} ions into the composite of ZrO_2 : Ho^{3+} coatings did not alter the overall shapes of the PL spectra, however, the intensity of the wideband derived from the zirconia matrix and PL bands related to f–f transition of Ho^{3+} ions were enhanced by raising the incorporation of Yb^{3+} ions into the composite coatings. This behavior was an indication of the role of Yb^{3+} ions in transmitting energy to Ho^{3+} ions [78,86].

Ćirić and Stojadinović also produced the ZrO_2 coating with Pr^{3+} incorporated particles [76]. Accordingly, they found that increasing the treatment time of the PEO process also increased the incorporation of uniformly distributed Pr^{3+} in the composite coating, where its contribution concurrently stabilized the tetragonal zirconia phase. They categorized PL emission spectral features into two distinct regions, including a broad PL band centered at approximately 495 nm and secondly a region due to the 4f–4f transitions of Pr^{3+} , where the most intense one was from the $^1D_2 \rightarrow ^3H_4$ transition [76]. The same authors reported fabrication of doped composite zirconia coatings containing Tm^{3+} and Yb^{3+} using the PEO process [75]. Tm and Yb particles promoted phase transformation from monoclinic to tetragonal phase, where the PL excitation spectra were identified by the broad band of ZrO_2 centered at approximately 280 nm and a peak at approximately 359 nm related to the $^3H_6 \rightarrow ^1D_2$ transition of Tm^{3+} .

6. Concluding Remarks and Future Outlook

The PEO coatings have various applications upon the preparation process and zirconium substrate. Several methods have already been implemented to improve bioresponse and antibacterial activity on the Zr surface. Until now, the PEO process has demonstrated promising results in reducing the risks associated with using the PEO coated Zr. Particularly, medical implants demand significant surface biocompatibility, which bare zirconium cannot meet for certain criteria. The rough and porous surface of PEO coatings stimulates nucleation and growth of biocompatible hydroxyapatite compounds due to offering a larger available surface for ionic interactions. The formation of PEO coatings reduces bacterial adhesion, and the incorporation of antibacterial agents, such as silver ions, provides a greater antibacterial feature. Incorporation of Zn and Cu ions in the PEO coating enhances the biocompatibility of coatings, where a more uniform and compact hydroxyapatite forms on the surface of coatings after prolonged immersion in the simulated body fluid.

PEO coating can enhance the corrosion protection of zirconium when immersed in aggressive media. The coatings were able to block the penetration paths of aggressive ions and enhanced the endurance of the zirconium substrate. The PEO coating also reduced the coefficient of friction and offered greater protection against sliding wear, as the debris released from the coatings usually acted as lubrication. Besides, the PEO composite coating with rare-earth elements offered tuning photoluminescence features of the zirconia, where the addition of different rare earth oxides could tailor the excitation and emission range of composite zirconia oxide.

On account of reviewed studies, the following remarks can be suggested for future studies:

- Inducing new nanoparticles in electrolytes during the PEO process opens a new path
 for future research, where there is a lack of studies on biomedical applications of Zr
 and Zr-alloys, such as enhancing the coatings' bioresponse and efficient delivering
 drugs to the body tissues.
- Poor surface features such as numerous pores and cracks confine the protection mechanism to the barrier inhibition, in which the coating halts the penetration of aggressive ions. However, producing composite coatings with protective agents such as sacrificing anodic nanoparticles can endow active protection to the substrates.

Coatings 2021, 11, 620 15 of 18

Wear behavior of coatings requires significant improvements. Besides, the wear mechanism of the coating has not been studied comprehensively. Using the PEO coated Zr-alloys in nuclear industries and applications demanding significant protection against fretting wear and corrosion requires more studies with simulated conditions.

 Tuning ZrO₂ bandgap for photocatalytic applications can draw attention to producing composite coatings with versatile applicability in splitting water and other compounds.

Author Contributions: C.V.R. conceived and supervised this work. N.A. collected all the data, obtained permission to use the data existing in the literature, and compiled the scientific validations. Both authors involved in preparing the manuscript. Both authors have read and agreed to the published version of the manuscript.

Funding: The authors also acknowledge, with pleasure, support from the National Science Foundation (NSF) with NSF-PREM grant #DMR-1827745.

Acknowledgments: NA acknowledges with pleasure the technical support and encouragement provided by the Center for Advanced Materials Research (CMR), UTEP. NA also acknowledges the Research Associate opportunity provided by CMR, UTEP.

Conflicts of Interest: The authors declare no conflict of interest.

References

- 1. Fattah-alhosseini, A.; Molaei, M.; Attarzadeh, N.; Babaei, K.; Attarzadeh, F. On the Enhanced Antibacterial Activity of Plasma Electrolytic Oxidation (PEO) Coatings That Incorporate Particles: A Review. *Ceram. Int.* **2020**, *46*, 20587–20607. [CrossRef]
- 2. Fattah-alhosseini, A.; Molaei, M.; Babaei, K. The Effects of Nano- and Micro-Particles on Properties of Plasma Electrolytic Oxidation (PEO) Coatings Applied on Titanium Substrates: A Review. Surf. Interfaces 2020, 21, 100659. [CrossRef]
- 3. Molaei, M.; Attarzadeh, N.; Fattah-alhosseini, A. Tailoring the Biological Response of Zirconium Implants Using Zirconia Bioceramic Coatings: A Systematic Review. *J. Trace Elem. Med. Biol.* **2021**, *66*, 126756. [CrossRef]
- 4. Bordbar-Khiabani, A.; Yarmand, B.; Sharifi-Asl, S.; Mozafari, M. Improved Corrosion Performance of Biodegradable Magnesium in Simulated Inflammatory Condition via Drug-Loaded Plasma Electrolytic Oxidation Coatings. *Mater. Chem. Phys.* **2020**, 239, 122003. [CrossRef]
- 5. Wang, D.; Liu, X.; Wu, Y.; Han, H.; Yang, Z.; Su, Y.; Zhang, X.; Wu, G.; Shen, D. Evolution Process of the Plasma Electrolytic Oxidation (PEO) Coating Formed on Aluminum in an Alkaline Sodium Hexametaphosphate ((NaPO₃)₆) Electrolyte. *J. Alloy. Compd.* **2019**, 798, 129–143. [CrossRef]
- 6. Sankara Narayanan, T.S.N.; Park, I.S.; Lee, M.H. Strategies to Improve the Corrosion Resistance of Microarc Oxidation (MAO) Coated Magnesium Alloys for Degradable Implants: Prospects and Challenges. *Prog. Mater. Sci.* **2014**, *60*, 1–71. [CrossRef]
- 7. Li, Z.; Cai, Z.; Cui, X.-J.; Liu, R.; Yang, Z.; Zhu, M. Influence of Nanoparticle Additions on Structure and Fretting Corrosion Behavior of Micro-Arc Oxidation Coatings on Zirconium Alloy. *Surf. Coat. Technol.* **2021**, *410*, 126949. [CrossRef]
- 8. Li, Z.; Cai, Z.; Ding, Y.; Cui, X.-J.; Yang, Z.; Zhu, M. Characterization of Graphene Oxide/ZrO₂ Composite Coatings Deposited on Zirconium Alloy by Micro-Arc Oxidation. *Appl. Surf. Sci.* **2020**, *506*, 144928. [CrossRef]
- 9. Arun, S.; Arunnellaiappan, T.; Rameshbabu, N. Fabrication of the Nanoparticle Incorporated PEO Coating on Commercially Pure Zirconium and Its Corrosion Resistance. *Surf. Coat. Technol.* **2016**, *305*, 264–273. [CrossRef]
- 10. Qin, W.; Nam, C.; Li, H.L.; Szpunar, J.A. Tetragonal Phase Stability in ZrO₂ Film Formed on Zirconium Alloys and Its Effects on Corrosion Resistance. *Acta Mater.* **2007**, *55*, 1695–1701. [CrossRef]
- 11. Cheng, Y.; Matykina, E.; Arrabal, R.; Skeldon, P.; Thompson, G.E. Plasma Electrolytic Oxidation and Corrosion Protection of Zircaloy-4. *Surf. Coat. Technol.* **2012**, 206, 3230–3239. [CrossRef]
- 12. Sandhyarani, M.; Rameshbabu, N.; Venkateswarlu, K.; Sreekanth, D.; Subrahmanyam, C. Surface Morphology, Corrosion Resistance and in Vitro Bioactivity of P Containing ZrO₂ Films Formed on Zr by Plasma Electrolytic Oxidation. *J. Alloy. Compd.* **2013**, 553, 324–332. [CrossRef]
- 13. Yan, Y.; Han, Y.; Li, D.; Huang, J.; Lian, Q. Effect of NaAlO₂ Concentrations on Microstructure and Corrosion Resistance of Al₂O₃/ZrO₂ Coatings Formed on Zirconium by Micro-Arc Oxidation. *Appl. Surf. Sci.* **2010**, 256, 6359–6366. [CrossRef]
- 14. Gefen, A. Optimizing the Biomechanical Compatibility of Orthopedic Screws for Bone Fracture Fixation. *Med. Eng. Phys.* **2002**, 24, 337–347. [CrossRef]
- 15. Thomsen, P.; Larsson, C.; Ericson, L.E.; Sennerby, L.; Lausmaa, J.; Kasemo, B. Structure of the Interface between Rabbit Cortical Bone and Implants of Gold, Zirconium and Titanium. *J. Mater. Sci. Mater. Med.* 1997, *8*, 653–665. [CrossRef] [PubMed]
- 16. Liu, Y.-T.; Lee, T.-M.; Lui, T.-S. Enhanced Osteoblastic Cell Response on Zirconia by Bio-Inspired Surface Modification. *Colloids Surf. B Biointerfaces* **2013**, *106*, 37–45. [CrossRef] [PubMed]
- 17. Wang, L.; Hu, X.; Nie, X. Deposition and Properties of Zirconia Coatings on a Zirconium Alloy Produced by Pulsed DC Plasma Electrolytic Oxidation. *Surf. Coat. Technol.* **2013**, 221, 150–157. [CrossRef]

Coatings 2021, 11, 620 16 of 18

18. Sanchez, A.G.; Schreiner, W.; Duffó, G.; Ceré, S. Surface Characterization of Anodized Zirconium for Biomedical Applications. Appl. Surf. Sci. 2011, 257, 6397–6405. [CrossRef]

- 19. Zhou, F.Y.; Wang, B.L.; Qiu, K.J.; Li, H.F.; Li, L.; Zheng, Y.F.; Han, Y. In Vitro Corrosion Behavior and Cellular Response of Thermally Oxidized Zr–3Sn Alloy. *Appl. Surf. Sci.* **2013**, 265, 878–888. [CrossRef]
- 20. Brenier, R.; Mugnier, J.; Mirica, E. XPS Study of Amorphous Zirconium Oxide Films Prepared by Sol–Gel. *Appl. Surf. Sci.* 1999, 143, 85–91. [CrossRef]
- 21. Leushake, U.; Krell, T.; Schulz, U.; Peters, M.; Kaysser, W.A.; Rabin, B.H. Microstructure and Phase Stability of EB-PVD Alumina and Alumina/Zirconia for Thermal Barrier Coating Applications. *Surf. Coat. Technol.* **1997**, 94–95, 131–136. [CrossRef]
- 22. Shanmugavelayutham, G.; Yano, S.; Kobayashi, A. Microstructural Characterization and Properties of ZrO₂/Al₂O₃ Thermal Barrier Coatings by Gas Tunnel-Type Plasma Spraying. *Vacuum* **2006**, *80*, 1336–1340. [CrossRef]
- Zhang, Z.; Wang, K.; Bai, C.; Li, X.; Dang, X.; Zhang, C. The Influence of UV Irradiation on the Biological Properties of MAO-Formed ZrO₂. Colloids Surf. B Biointerfaces 2012, 89, 40–47. [CrossRef]
- Sandhyarani, M.; Prasadrao, T.; Rameshbabu, N. Role of Electrolyte Composition on Structural, Morphological and in-Vitro Biological Properties of Plasma Electrolytic Oxidation Films Formed on Zirconium. Appl. Surf. Sci. 2014, 317, 198–209. [CrossRef]
- 25. Han, Y.; Yan, Y.; Lu, C. Ultraviolet-Enhanced Bioactivity of ZrO₂ Films Prepared by Micro-Arc Oxidation. *Thin Solid Film*. **2009**, 517, 1577–1581. [CrossRef]
- 26. Han, Y.; Yan, Y.; Lu, C.; Zhang, Y.; Xu, K. Bioactivity and Osteoblast Response of the Micro-Arc Oxidized Zirconia Films. *J. Biomed. Mater. Res. Part A* **2009**, 88A, 117–127. [CrossRef] [PubMed]
- 27. Yan, Y.; Han, Y.; Lu, C. The Effect of Chemical Treatment on Apatite-Forming Ability of the Macroporous Zirconia Films Formed by Micro-Arc Oxidation. *Appl. Surf. Sci.* **2008**, 254, 4833–4839. [CrossRef]
- 28. Zhang, L.; Zhu, S.; Han, Y.; Xiao, C.; Tang, W. Formation and Bioactivity of HA Nanorods on Micro-Arc Oxidized Zirconium. *Mater. Sci. Eng. C* **2014**, *43*, 86–91. [CrossRef] [PubMed]
- 29. Cengiz, S.; Uzunoglu, A.; Stanciu, L.; Tarakci, M.; Gencer, Y. Direct Fabrication of Crystalline Hydroxyapatite Coating on Zirconium by Single-Step Plasma Electrolytic Oxidation Process. *Surf. Coat. Technol.* **2016**, *301*, 74–79. [CrossRef]
- 30. Surmenev, R.A.; Surmeneva, M.A.; Ivanova, A.A. Significance of Calcium Phosphate Coatings for the Enhancement of New Bone Osteogenesis—A Review. *Acta Biomater.* **2014**, *10*, 557–579. [CrossRef] [PubMed]
- 31. Viswanath, B.; Ravishankar, N. Controlled Synthesis of Plate-Shaped Hydroxyapatite and Implications for the Morphology of the Apatite Phase in Bone. *Biomaterials* **2008**, *29*, 4855–4863. [CrossRef]
- 32. Roy, M.; Bandyopadhyay, A.; Bose, S. Induction Plasma Sprayed Nano Hydroxyapatite Coatings on Titanium for Orthopaedic and Dental Implants. *Surf. Coat. Technol.* **2011**, 205, 2785–2792. [CrossRef] [PubMed]
- 33. Lu, S.-F.; Lou, B.-S.; Yang, Y.-C.; Wu, P.-S.; Chung, R.-J.; Lee, J.-W. Effects of Duty Cycle and Electrolyte Concentration on the Microstructure and Biocompatibility of Plasma Electrolytic Oxidation Treatment on Zirconium Metal. *Thin Solid Film.* **2015**, 596, 87–93. [CrossRef]
- 34. Bayati, M.R.; Aminzare, M.; Molaei, R.; Sadrnezhaad, S.K. Micro Arc Oxidation of Nano-Crystalline Ag-Doped TiO₂ Semiconductors. *Mater. Lett.* **2011**, *65*, 840–842. [CrossRef]
- 35. Teker, D.; Muhaffel, F.; Menekse, M.; Karaguler, N.G.; Baydogan, M.; Cimenoglu, H. Characteristics of Multi-Layer Coating Formed on Commercially Pure Titanium for Biomedical Applications. *Mater. Sci. Eng. C* **2015**, *48*, 579–585. [CrossRef]
- 36. Fidan, S.; Muhaffel, F.; Riool, M.; Cempura, G.; de Boer, L.; Zaat, S.A.J.; Filemonowicz, A.C.; Cimenoglu, H. Fabrication of Oxide Layer on Zirconium by Micro-Arc Oxidation: Structural and Antimicrobial Characteristics. *Mater. Sci. Eng. C* 2017, 71, 565–569. [CrossRef]
- 37. Durdu, S.; Aktug, S.L.; Aktas, S.; Yalcin, E.; Cavusoglu, K.; Altinkok, A.; Usta, M. Characterization and in Vitro Properties of Antibacterial Ag-Based Bioceramic Coatings Formed on Zirconium by Micro Arc Oxidation and Thermal Evaporation. *Surf. Coat. Technol.* **2017**, 331, 107–115. [CrossRef]
- 38. Aktuğ, S.L.; Durdu, S.; Yalçın, E.; Çavuşoğlu, K.; Usta, M. In Vitro Properties of Bioceramic Coatings Produced on Zirconium by Plasma Electrolytic Oxidation. *Surf. Coat. Technol.* **2017**, 324, 129–139. [CrossRef]
- 39. Aktug, S.L.; Kutbay, I.; Usta, M. Characterization and Formation of Bioactive Hydroxyapatite Coating on Commercially Pure Zirconium by Micro Arc Oxidation. *J. Alloy. Compd.* **2017**, 695, 998–1004. [CrossRef]
- 40. Cengiz, S.; Azakli, Y.; Tarakci, M.; Stanciu, L.; Gencer, Y. Microarc Oxidation Discharge Types and Bio Properties of the Coating Synthesized on Zirconium. *Mater. Sci. Eng. C* **2017**, *77*, 374–383. [CrossRef]
- 41. Sandhyarani, M.; Rameshbabu, N.; Venkateswarlu, K. Fabrication, Characterization and in-Vitro Evaluation of Nanostructured Zirconia/Hydroxyapatite Composite Film on Zirconium. *Surf. Coat. Technol.* **2014**, 238, 58–67. [CrossRef]
- 42. Durdu, S.; Aktug, S.L.; Aktas, S.; Yalcin, E.; Usta, M. Fabrication and in Vitro Properties of Zinc-Based Superhydrophilic Bioceramic Coatings on Zirconium. *Surf. Coat. Technol.* **2018**, *344*, 467–478. [CrossRef]
- 43. Zhang, L.; Han, Y.; Tan, G. Hydroxyaptite Nanorods Patterned ZrO2 Bilayer Coating on Zirconium for the Application of Percutaneous Implants. *Colloids Surf. B Biointerfaces* **2015**, 127, 8–14. [CrossRef]
- 44. Aktug, S.L.; Durdu, S.; Aktas, S.; Yalcin, E.; Usta, M. Characterization and Investigation of in Vitro Properties of Antibacterial Copper Deposited on Bioactive ZrO₂ Coatings on Zirconium. *Thin Solid Film.* **2019**, *681*, 69–77. [CrossRef]
- 45. Cengiz, S.; Uzunoglu, A.; Huang, S.M.; Stanciu, L.; Tarakci, M.; Gencer, Y. An In-Vitro Study: The Effect of Surface Properties on Bioactivity of the Oxide Layer Fabricated on Zr Substrate by PEO. *Surf. Interfaces* **2021**, 22, 100884. [CrossRef]

Coatings 2021, 11, 620 17 of 18

46. Motta, A.T.; Yilmazbayhan, A.; da Silva, M.J.G.; Comstock, R.J.; Was, G.S.; Busby, J.T.; Gartner, E.; Peng, Q.; Jeong, Y.H.; Park, J.Y. Zirconium Alloys for Supercritical Water Reactor Applications: Challenges and Possibilities. *J. Nucl. Mater.* **2007**, *371*, 61–75. [CrossRef]

- 47. Yau, T.-L.; Annamalai, V.E. Corrosion of Zirconium and its Alloys. In *Reference Module in Materials Science and Materials Engineering*; Elsevier: Amsterdam, The Netherlands, 2016; ISBN 978-0-12-803581-8.
- 48. Yau, T.-L.; Sutherlin, R.C.; Chang, A.T.I.W. Corrosion of Zirconium and Zirconium Alloys. In *Corrosion: Materials*; Stephen, D.C., Bernard, S.C., Eds.; ASM International: Ohio, OH, USA, 2018; Chapter 20, pp. 300–324.
- 49. Chen, Y.; Nie, X.; Northwood, D.O. Investigation of Plasma Electrolytic Oxidation (PEO) Coatings on a Zr–2.5Nb Alloy Using High Temperature/Pressure Autoclave and Tribological Tests. *Surf. Coat. Technol.* **2010**, 205, 1774–1782. [CrossRef]
- 50. Cheng, Y.; Wu, F. Plasma Electrolytic Oxidation of Zircaloy-4 Alloy with DC Regime and Properties of Coatings. *Trans. Nonferrous Met. Soc. China* **2012**, 22, 1638–1646. [CrossRef]
- 51. Cheng, Y.; Wu, F.; Matykina, E.; Skeldon, P.; Thompson, G.E. The Influences of Microdischarge Types and Silicate on the Morphologies and Phase Compositions of Plasma Electrolytic Oxidation Coatings on Zircaloy-2. *Corros. Sci.* **2012**, *59*, 307–315. [CrossRef]
- 52. Sreekanth, D.; Rameshbabu, N.; Venkateswarlu, K. Effect of Various Additives on Morphology and Corrosion Behavior of Ceramic Coatings Developed on AZ31 Magnesium Alloy by Plasma Electrolytic Oxidation. *Ceram. Int.* **2012**, *38*, 4607–4615. [CrossRef]
- 53. Cheng, Y.; Wu, F.; Dong, J.; Wu, X.; Xue, Z.; Matykina, E.; Skeldon, P.; Thompson, G.E. Comparison of Plasma Electrolytic Oxidation of Zirconium Alloy in Silicate- and Aluminate-Based Electrolytes and Wear Properties of the Resulting Coatings. *Electrochim. Acta* 2012, 85, 25–32. [CrossRef]
- 54. Cheng, Y.; Cao, J.; Peng, Z.; Wang, Q.; Matykina, E.; Skeldon, P.; Thompson, G.E. Wear-Resistant Coatings Formed on Zircaloy-2 by Plasma Electrolytic Oxidation in Sodium Aluminate Electrolytes. *Electrochim. Acta* **2014**, *116*, 453–466. [CrossRef]
- 55. Trivinho-Strixino, F.; da Silva, D.X.; Paiva-Santos, C.O.; Pereira, E.C. Tetragonal to Monoclinic Phase Transition Observed during Zr Anodisation. *J. Solid State Electrochem.* **2013**, *17*, 191–199. [CrossRef]
- 56. Zou, Z.; Xue, W.; Jia, X.; Du, J.; Wang, R.; Weng, L. Effect of Voltage on Properties of Microarc Oxidation Films Prepared in Phosphate Electrolyte on Zr–1Nb Alloy. *Surf. Coat. Technol.* **2013**, 222, 62–67. [CrossRef]
- 57. Xue, W.; Zhu, Q.; Jin, Q.; Hua, M. Characterization of Ceramic Coatings Fabricated on Zirconium Alloy by Plasma Electrolytic Oxidation in Silicate Electrolyte. *Mater. Chem. Phys.* **2010**, *120*, 656–660. [CrossRef]
- 58. Sukumaran, A.; Sampatirao, H.; Balasubramanian, R.; Parfenov, E.; Mukaeva, V.; Nagumothu, R. Formation of ZrO₂–SiC Composite Coating on Zirconium by Plasma Electrolytic Oxidation in Different Electrolyte Systems Comprising of SiC Nanoparticles. *Trans. Inst. Met.* **2018**, *71*, 1699–1713. [CrossRef]
- 59. Wang, Y.M.; Feng, W.; Xing, Y.R.; Ge, Y.L.; Guo, L.X.; Ouyang, J.H.; Jia, D.C.; Zhou, Y. Degradation and Structure Evolution in Corrosive LiOH Solution of Microarc Oxidation Coated Zircaloy-4 Alloy in Silicate and Phosphate Electrolytes. *Appl. Surf. Sci.* **2018**, *431*, 2–12. [CrossRef]
- Wu, J.; Lu, P.; Dong, L.; Zhao, M.; Li, D.; Xue, W. Combination of Plasma Electrolytic Oxidation and Pulsed Laser Deposition for Preparation of Corrosion-Resisting Composite Film on Zirconium Alloys. *Mater. Lett.* 2020, 262, 127080. [CrossRef]
- 61. Yilmazbayhan, A.; Motta, A.T.; Comstock, R.J.; Sabol, G.P.; Lai, B.; Cai, Z. Structure of Zirconium Alloy Oxides Formed in Pure Water Studied with Synchrotron Radiation and Optical Microscopy: Relation to Corrosion Rate. *J. Nucl. Mater.* **2004**, 324, 6–22. [CrossRef]
- 62. Raj, B.; Mudali, U.K. Materials Development and Corrosion Problems in Nuclear Fuel Reprocessing Plants. *Prog. Nucl. Energy* **2006**, *48*, 283–313. [CrossRef]
- 63. Fisher, N.J.; Weckwerth, M.K.; Grandison, D.A.E.; Cotnam, B.M. Fretting-Wear of Zirconium Alloys. *Nucl. Eng. Des.* **2002**, 213, 79–90. [CrossRef]
- 64. Helmi Attia, M. On the Fretting Wear Mechanism of Zr-Alloys. Tribol. Int. 2006, 39, 1320–1326. [CrossRef]
- 65. Cheng, Y.; Xue, Z.; Wang, Q.; Wu, X.-Q.; Matykina, E.; Skeldon, P.; Thompson, G.E. New Findings on Properties of Plasma Electrolytic Oxidation Coatings from Study of an Al–Cu–Li Alloy. *Electrochim. Acta* **2013**, *107*, 358–378. [CrossRef]
- 66. Martini, C.; Ceschini, L.; Tarterini, F.; Paillard, J.M.; Curran, J.A. PEO Layers Obtained from Mixed Aluminate–Phosphate Baths on Ti–6Al–4V: Dry Sliding Behaviour and Influence of a PTFE Topcoat. *Wear* **2010**, 269, 747–756. [CrossRef]
- 67. Yan, Y.; Han, Y.; Huang, J. Formation of Al₂O₃–ZrO₂ Composite Coating on Zirconium by Micro-Arc Oxidation. *Scr. Mater.* **2008**, 59, 203–206. [CrossRef]
- 68. Zhang, L.; Zhang, W.; Han, Y.; Tang, W. A Nanoplate-like α-Al₂O₃ out-Layered Al₂O₃-ZrO₂ Coating Fabricated by Micro-Arc Oxidation for Hip Joint Prosthesis. *Appl. Surf. Sci.* **2016**, *361*, 141–149. [CrossRef]
- 69. Wei, K.; Chen, L.; Qu, Y.; Yu, J.; Jin, X.; Du, J.; Xue, W.; Zhang, J. Tribological Properties of Microarc Oxidation Coatings on Zirlo Alloy. *Surf. Eng.* **2019**, *35*, 692–700. [CrossRef]
- 70. Atuchin, V.V.; Aliev, V.S.; Kruchinin, V.N.; Ramana, C.V. Optical Properties of ZrO₂ Films Fabricated by Ion Beam Sputtering Deposition at Low Temperature. In Proceedings of the 2007 International Forum on Strategic Technology, Ulaanbaatar, Mongolia, 3–6 October 2007; pp. 529–531.

Coatings 2021, 11, 620 18 of 18

71. Ramana, C.V.; Utsunomiya, S.; Ewing, R.C.; Becker, U.; Atuchin, V.V.; Aliev, V.S.; Kruchinin, V.N. Spectroscopic Ellipsometry Characterization of the Optical Properties and Thermal Stability of ZrO₂ Films Made by Ion-Beam Assisted Deposition. *Appl. Phys. Lett.* **2008**, 92, 11917. [CrossRef]

- 72. Ramana, C.V.; Vemuri, R.S.; Fernandez, I.; Campbell, A.L. Size-Effects on the Optical Properties of Zirconium Oxide Thin Films. *Appl. Phys. Lett.* **2009**, *95*, 231905. [CrossRef]
- 73. Noor-A-Alam, M.; Ramana, C.; Choudhuri, A. Analysis of microstructure and thermal stability of hafnia-zirconia based thermal barrier coatings. In Proceedings of the 9th Annual International Energy Conversion Engineering Conference, International Energy Conversion Engineering Conference (IECEC), San Diego, CA, USA, 31 July–3 August 2011.
- 74. Lokesha, H.S.; Nagabhushana, K.R.; Chithambo, M.L.; Singh, F. Down and Upconversion Photoluminescence of ZrO₂:Er³⁺ Phosphor Irradiated with 120 MeV Gold Ions. *Mater. Res. Express* **2020**, *7*, 64006. [CrossRef]
- 75. Ćirić, A.; Stojadinović, S. Photoluminescence Studies of ZrO2:Tm³⁺/Yb³⁺ Coatings Formed by Plasma Electrolytic Oxidation. *J. Lumin.* **2019**, 214, 116568. [CrossRef]
- 76. Ćirić, A.; Stojadinović, S. Photoluminescence Properties of Pr³⁺ Doped ZrO₂ Formed by Plasma Electrolytic Oxidation. *J. Alloy. Compd.* **2019**, 803, 126–134. [CrossRef]
- 77. Stojadinović, S.; Tadić, N.; Vasilić, R. Photoluminescence Properties of Er³⁺/Yb³⁺ Doped ZrO₂ Coatings Formed by Plasma Electrolytic Oxidation. *J. Lumin.* **2019**, 208, 296–301. [CrossRef]
- 78. Stojadinović, S.; Tadić, N.; Vasilić, R. Down- and up-Conversion Photoluminescence of ZrO2:Ho³⁺ and ZrO2:Ho³⁺ /Yb³⁺ Coatings Formed by Plasma Electrolytic Oxidation. *J. Alloy. Compd.* **2019**, 785, 1222–1232. [CrossRef]
- 79. Stojadinović, S.; Tadić, N.; Vasilić, R. Down-Conversion Photoluminescence of ZrO2:Er³⁺ Coatings Formed by Plasma Electrolytic Oxidation. *Mater. Lett.* **2018**, 219, 251–255. [CrossRef]
- 80. Stojadinović, S.; Tadić, N.; Vasilić, R. Structural and Photoluminescent Properties of ZrO2:Tb³⁺ Coatings Formed by Plasma Electrolytic Oxidation. *J. Lumin.* **2018**, *197*, 83–89. [CrossRef]
- 81. Stojadinović, S.; Tadić, N.; Vasilić, R. Photoluminescence of Sm³⁺ Doped ZrO₂ Coatings Formed by Plasma Electrolytic Oxidation of Zirconium. *Mater. Lett.* **2016**, *164*, 329–332. [CrossRef]
- 82. Stojadinović, S.; Vasilić, R.; Radić, N.; Grbić, B. Zirconia Films Formed by Plasma Electrolytic Oxidation: Photoluminescent and Photocatalytic Properties. *Opt. Mater.* **2015**, *40*, 20–25. [CrossRef]
- 83. Cao, H.; Qiu, X.; Luo, B.; Liang, Y.; Zhang, Y.; Tan, R.; Zhao, M.; Zhu, Q. Synthesis and Room-Temperature Ultraviolet Photoluminescence Properties of Zirconia Nanowires. *Adv. Funct. Mater.* **2004**, 14, 243–246. [CrossRef]
- 84. Cong, Y.; Li, B.; Yue, S.; Fan, D.; Wang, X.J. Effect of Oxygen Vacancy on Phase Transition and Photoluminescence Properties of Nanocrystalline Zirconia Synthesized by the One Pot Reaction. *J. Phys. Chem. C* **2009**, *113*, 13974–13978. [CrossRef]
- 85. Kumari, L.; Li, W.Z.; Xu, J.M.; Leblanc, R.M.; Wang, D.Z.; Li, Y.; Guo, H.; Zhang, J. Controlled Hydrothermal Synthesis of Zirconium Oxide Nanostructures and Their Optical Properties. *Cryst. Growth Des.* **2009**, *9*, 3874–3880. [CrossRef]
- 86. Jain, N.; Singh, R.K.; Sinha, S.; Singh, R.A.; Singh, J. Color Tunable Emission through Energy Transfer from Yb³⁺ Co-Doped SrSnO₃:Ho³⁺ Perovskite Nano-Phosphor. *Appl. Nanosci.* **2018**, *8*, 1267–1278. [CrossRef]